Journal of the Ceramic Society of Japan 132 [7] 387-396 2024
DOI https://doi.org/10.2109/jcersj2.24023

JCS-Japan

SPECIAL ARTICLE-ACADEMIC ACHIEVEMENTS

The 67th CerSJ Awards for Academic Achievements in Ceramic Science and Technology: Review

Colloidal formation process based on electrophoretic phenomena of charged particles in liquid media and electrode reactions

Tetsuo Uchikoshi[1,†]

[1]National Institute for Materials Science, 1–2–1 Sengen, Tsukuba, Ibaraki 305–0047, Japan

The electrophoresis of particles by applying an electric field to a colloidal suspension allows the simultaneous manipulation and shaping of particles. A film forming process utilizing the electrophoretic phenomenon of charged particles in a liquid is called "electrophoretic deposition (EPD)" and is used for powder coating. The main difference between the EPD process and other colloidal processes is the coexistence of electrode reactions, i.e., electrochemical reactions that occur at the interface between the electrode and the electrolyte solution. The applied electric field in the EPD method plays an important role not only in the electrophoresis of charged particles but also in controlling the coagulation mechanism and film quality. This paper introduces the principle of the EPD process considering the electrode reaction and an example of the functional film formation process.

Key-words : Electrophoretic deposition, Electrode reaction, Colloidal suspension, Coating, Binder

[Received March 10, 2024; Accepted April 23, 2024; Published online May 30, 2024]

1. Introduction

A colloid is a state in which a certain substance is dispersed within another substance in the form of particles within a specific size range (about 10^{-7} to 10^{-9} m). Colloidal particles dispersed in a liquid are larger than solute molecules or ions and are electrically charged, so they exhibit unique properties such as Brownian motion, Tyndall phenomenon, dialysis, and electrophoresis. In addition, colloidal particles coagulate and salt out in the presence of electrolytes. The fundamental properties of these colloidal particles are determined by their particle size, regardless of the type of material. Therefore, when submicron to nanosized particles of any material are dispersed in a liquid, such as water or a nonaqueous solvent, they exhibit characteristics common to colloidal particles. Taking Brownian motion as an example, if the temperature and viscosity of the dispersion medium are constant, the movement of particles does not depend on the type of substance, but only on the size of the particles; the movement is faster for smaller particles and slower for larger particles. By utilizing this property of colloidal particles, the speed of Brownian motion and particle size can be measured from the change in scattering intensity when the particles are irradiated with laser light. Furthermore, if the particles are agglomerated from a suspension of colloidal particles using the appropriate method, a dense solidified body can be obtained. A powder compaction method using a suspension is called a colloidal process, and is widely used industrially as a method for producing ceramic products with complex shapes.[1)–5)] However, ensuring a high dispersibility and fluidity of particles in liquids requires optimization of the selection of solvents, dispersants, and binders, as well as the ionic strength and pH. Additionally, colloidal methods often take a long time to solidify particles in a suspension, making them less suitable for large-scale production than traditional dry molding methods. The advantage of the colloidal process is that it can produce solidified bodies with controlled microstructures by controlling the interaction of the attractive and repulsive forces between particles in the dispersion medium.

Typical solidification methods using the colloid process are shown in **Table 1**.[6)] Slip casting is the most widely used colloidal process. In this method, a solidified body can be produced by pouring the suspension into a porous mold having hygroscopic properties, such as plaster, and absorbing the solvent by capillary force. Centrifugal molding is a method that applies a centrifugal force to a slurry and causes particles in the liquid to settle in the direction of the centrifugal force. Tape casting is used to form a sheet-like compact from a suspension using the knife edge of a doctor blade onto a carrier film. Electrophoretic deposition (EPD)[7)–13)] is a method in which an electric field is applied to a suspension to cause charged particles to migrate and be deposited on a substrate, as shown in **Fig. 1**.[14)] Based on this method, the solidification rate is independent of the particle size and a dense deposited film can be obtained. Furthermore, the EPD method allows easy control of the film thickness and is also excellent for

† Corresponding author: T. Uchikoshi; E-mail: uchikoshi.tetsuo@nims.go.jp

Table 1. Classification of solidification methods in colloidal processes

Method	Acting force	Material	
		Stationary object	Moving object
Slip casting	Capillary force	Particle Ion	Solvent
Filtration under pressurization or decompression	Compression force Suction force	Particle Ion	Solvent
Centrifugal molding	Centrifugal force	Ion	Particle Solvent
Tape casting	Blade shear force Crosslinking force of polymer	Particle Ion Solvent	
Electrophoretic deposition	Electrohydrodynamic force Electrochemical force	Solvent	Particle Ion

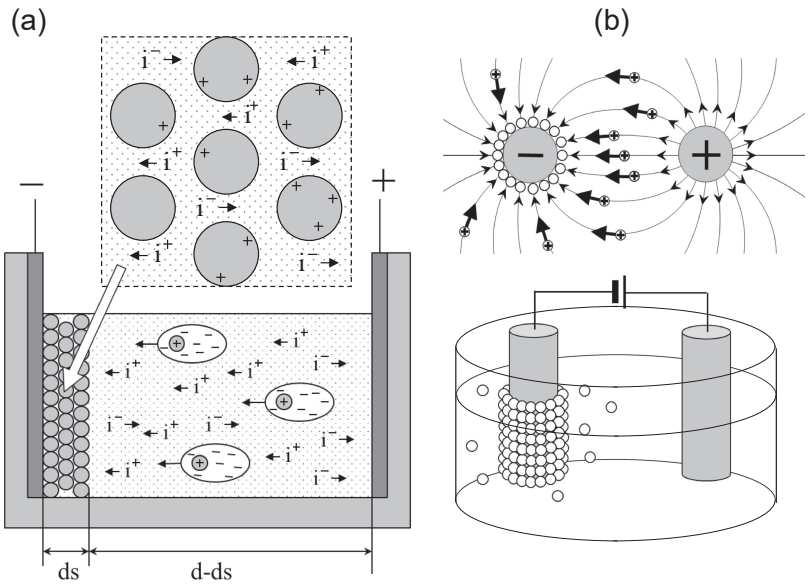

Fig. 1. Schematic diagram of electrophoresis process: (a) Electrophoresis and deposition of ions and particles in suspension; (b) Electric field lines between two cylindrical electrodes and particles migrating along the potential gradient in a solvent.

layered film formation. Furthermore, since the arrangement of particles can be controlled by applying an external field, such as a magnetic field, it is suitable for the advanced microstructure control of ceramics.[15)–20)] The major difference between the EPD method and other colloidal processes lies in the presence or absence of electrode reactions, that is, electrochemical reactions that occur at the interface between the electrode and the electrolyte solvent. The applied electric field in the EPD method not only controls the electrophoretic phenomenon of the charged particles, but also plays an important role in controlling the solidification mechanism and film quality. This article introduces the principles and application examples of the EPD process that takes the electrode reactions into consideration.

2. Electrode reaction and particle deposition during the EPD process

In the EPD process, particles, such as ceramics, are electrically charged and dispersed in a liquid, then an electric field is applied to the suspension. Particles are then electrophoresed in the direction of the electrode, which has a polarity different from the surface charge, to form a particle deposit layer on the electrode substrate. In suspensions used in the EPD processes, control of the charge state of particles is more important than in other colloidal processes. This is also related to the complexity of the particle deposition mechanism during the EPD.

According to Hamaker's mass balance law,[21)] the amount of particle deposition W (g) due to the electrophoretic process is expressed by the following formula.[13)]

$$\frac{dW}{dt} = f\mu CEA \tag{1}$$

where t is the deposition time (s), μ is the electrophoretic mobility (m^2/Vs), E is the potential gradient (V/m), C is the amount of the solid phase in the suspension (g/m^3), A is the electrode area. (m^2), and f is the "sticking parameter" or the adhesion probability of particles reaching the substrate ($0 \leq f \leq 1$).[7)] During the particle deposition process,

the potential gradient E changes, and the following equation holds between the circuit current I (A) and the suspension conductivity Λ (S/m).

$$E = \frac{I}{S\Lambda} \tag{2}$$

Furthermore, the potential V_a applied to the circuit is reduced by the potential drop at the anode and cathode and the ohmic loss at the suspension and solidified layer, so the following equation holds between them.

$$V_a = \Delta\phi_{anode} + IR_{sus}(d - d_s) + IR_s d_s + \Delta\phi_{cathode} \tag{3}$$

where $\Delta\phi_{anode}$ and $\Delta\phi_{cathode}$ are the potential drops at the anode and cathode, respectively, R_{sus} and R_s are the apparent resistances of the suspension and solidified layer (Ω/m), respectively, and d and d_s are the electrode distance and solidified layer thickness, respectively.

The sticking parameter f was introduced to explain the case when electrophoresis occurs but no or less deposition occurs, but its details have not been significantly discussed. The deposition phenomenon cannot be understood unless the particle electrophoresis step and the deposition step are treated as separate the phenomena.

Particle coagulation during the EPD process is understood as a powder agglomeration phenomenon according to the DLVO theory.[7),10)] In other words, in order for particles to accumulate on the electrode substrate, particles that reach the vicinity of the electrode must rapidly lose their surface charge, reduce their electrostatic repulsion potential, and aggregate on the substrate due to van der Waals forces. The roles of the applied electric field in the EPD process include (1) electrophoresis of the charged particles; (2) pressing charged particles which have not yet lost their charge onto the substrate by the force of the electric field after reaching the electrode, and (3) significantly changing the pH of the solvent near the electrode. In particular, it is important to pay attention to pH changes near the electrodes.[22)–25)]

Figure 2 shows a schematic diagram of the experiment conducted by us. A solvent prepared by adding nitric acid to commercially-available ethanol to adjust the pH to 4.5, and a suspension (zeta potential +50 mV) prepared by dispersing alumina powder in ethanol and adjusting the pH to 4.5 by adding nitric acid were prepared. A pair of stainless-steel plates were immersed, and a DC electric field of 20 V/cm was continuously applied or with ON/OFF DC pulses. The reason for using DC pulses was to control the pH changes near the electrodes, and to keep the amount of current flowing through the circuit constant regardless of the pulse frequency. The total ON time was set to 10 min. Next, at regular intervals after the start of the current application, a small amount of the solvent near the electrode was collected using a micropipette, and the pH was measured using an ion-sensitive field effect transistor (IS-FET) sensor.[23)] Additionally, the still-wet deposit on the cathode was sampled and the pH of the deposit was measured using the IS-FET sensor.

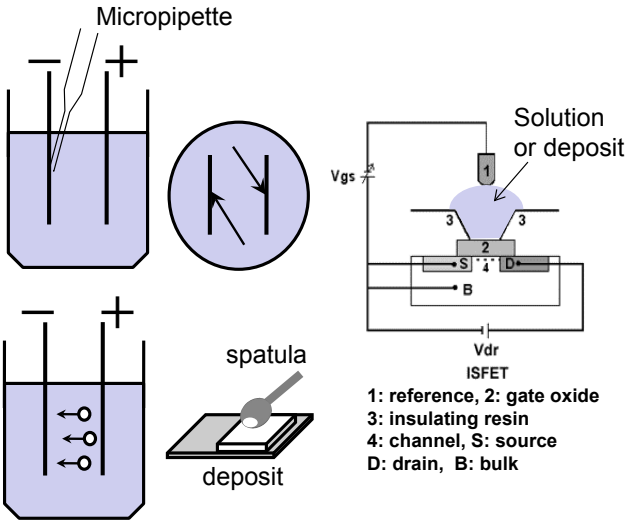

Fig. 2. Schematic diagram of pH change measurement near the electrode by applying an electric field.

Figure 3 shows the results. When the current was started, the pH of the solvent near the cathode significantly increased, and in contrast, the pH of the solvent near the anode slightly decreased. Furthermore, as the pulse interval became shorter, the pH change became smaller. It was confirmed that under the current conditions when the pH of the solvent significantly changed, a high amount of particles deposited on the cathode, and the pH in the deposited layer also increased. This is because the positively charged alumina particles in a suspension adjusted to pH 4.5 rapidly lost their electrostatic repulsion when they reach the area near the cathode substrate where the pH has increased to around 10–12, resulting in the agglomeration on the substrate due to the van der Waals attractive force.

The following various reactions are thought to be the cause of the pH near the cathode being largely biased toward the basic side when electricity is applied. These are commonly called cathodic reactions.

$$2H_2O + 2e^- \rightarrow H_2 + 2OH^- \tag{4}$$
$$O_2 + 2H_2O + 4e^- \rightarrow 4OH^- \tag{5}$$
$$NO_3^- + H_2O + 2e^- \rightarrow NO_2^- + 2OH^- \tag{6}$$
$$NO_3^- + 7H_2O + 8e^- \rightarrow NH_4^+ + 10OH^- \tag{7}$$
$$ClO_4^- + H_2O + 2e^- \rightarrow ClO_3^- + 2OH^- \tag{8}$$
$$ClO_4^- + 4H_2O + 8e^- \rightarrow Cl^- + 8OH^- \tag{9}$$
$$H_2O_2 + 2e^- \rightarrow 2OH^- \tag{10}$$

Cathodic reactions are significantly affected by the amount of impurity water contained in the solvent and the type of acid used, and the magnitude of the pH deviation varies depending on the suspension preparation conditions. Until now, it has been pointed out that there are many cases in which particles do not deposit on the electrode substrate even when electrophoretic phenomena are observed in various material systems, and it has even been said that the EPD process is material selective. However, by selecting the suspension preparation and electric field application conditions so that the pH change near the electrode

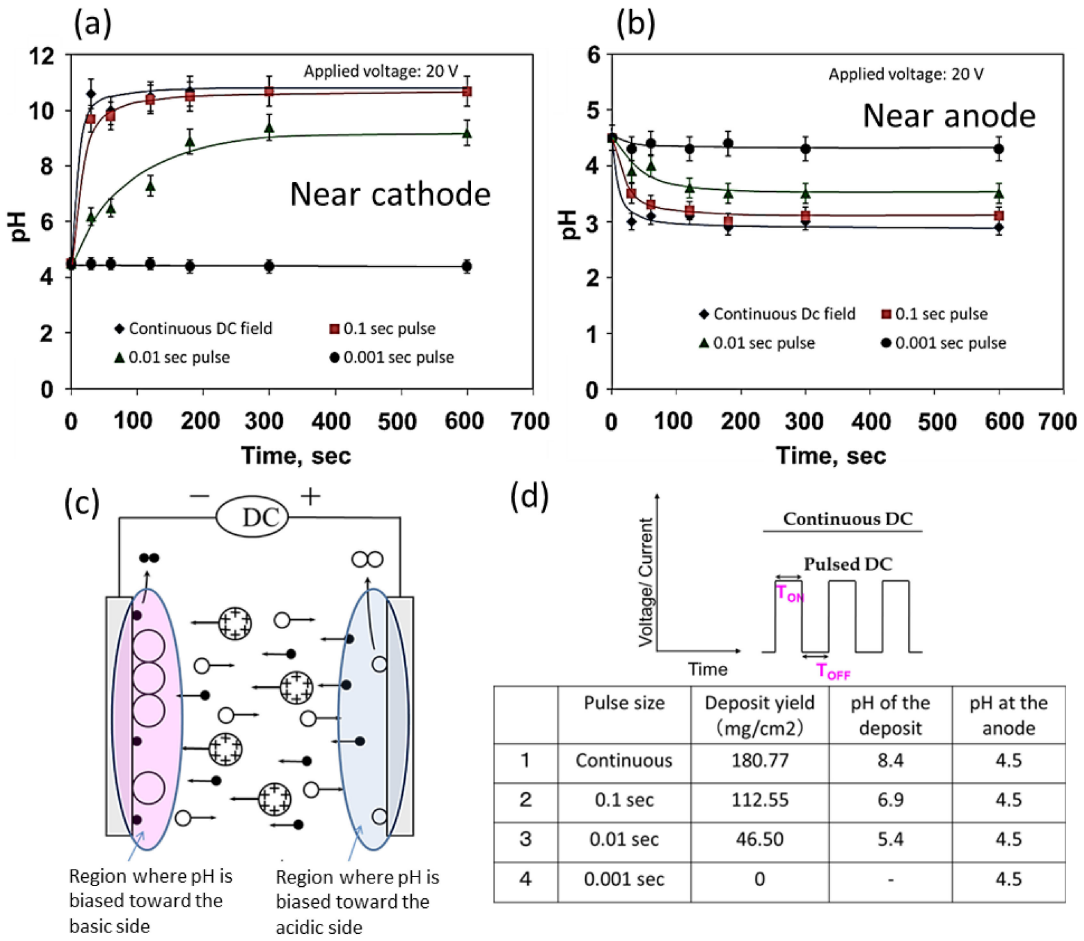

	Pulse size	Deposit yield (mg/cm2)	pH of the deposit	pH at the anode
1	Continuous	180.77	8.4	4.5
2	0.1 sec	112.55	6.9	4.5
3	0.01 sec	46.50	5.4	4.5
4	0.001 sec	0	-	4.5

Fig. 3. pH change of the solvent near the electrode due to the electrode reaction during electric field application, and pH of the cathode deposit after the cathode deposition of the alumina suspension: (a) and (b) pH of solvent with no particles added; (c) Schematic diagram of cathodic deposition of alumina suspension; (d) Deposit yield and pH after cathodic deposition of alumina suspension.

approaches the isoelectric point of the suspension, deposition can be achieved using various material systems, which was said to be difficult in the past. Thus, the application of the EPD process has significantly expanded.

Figure 4 shows the mechanism of particle deposition based on pH localization by the cathodic reactions. However, the adhesion force of as-deposited particles to the substrate due to the van der Waals forces and the bonding force between particles are not sufficiently high. It often requires the addition of organic binders, such as polyvinyl butyral (PVB), polyvinylpyrrolidone (PVP), or polyvinyl alcohol (PVA), followed by a heat treatment step for degreasing. Improving particle adhesion and bonding strength without the use of organic binders is a major challenge in the EPD processes, as the addition of binders often reduces the suspension stability and inhibits particle deposition. The addition of an organic binder is not sufficient to achieve a high adhesion of deposited films at room temperature and under as-deposition conditions. Therefore, it was necessary to develop a technology that enables strong particle–particle and particle-substrate bonding (coexistence of chemical reactions) at the same time when the EPD is completed.

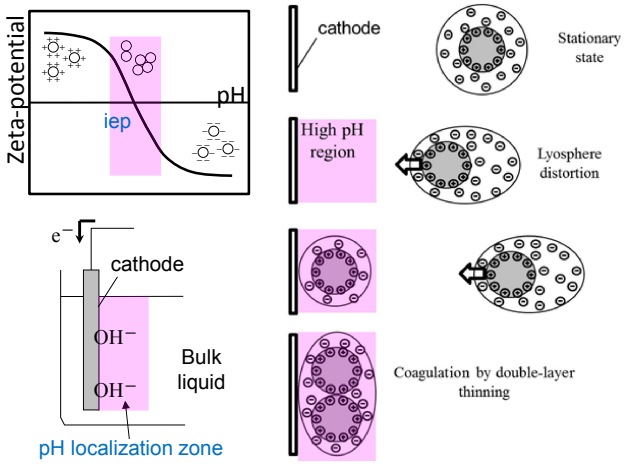

Fig. 4. Deposition mechanism based on pH localization by cathodic electrode reaction.

3. Unfired ceramic coating using the EPD process

As already mentioned, when cathodic deposition is performed with a positively charged suspension of particles,

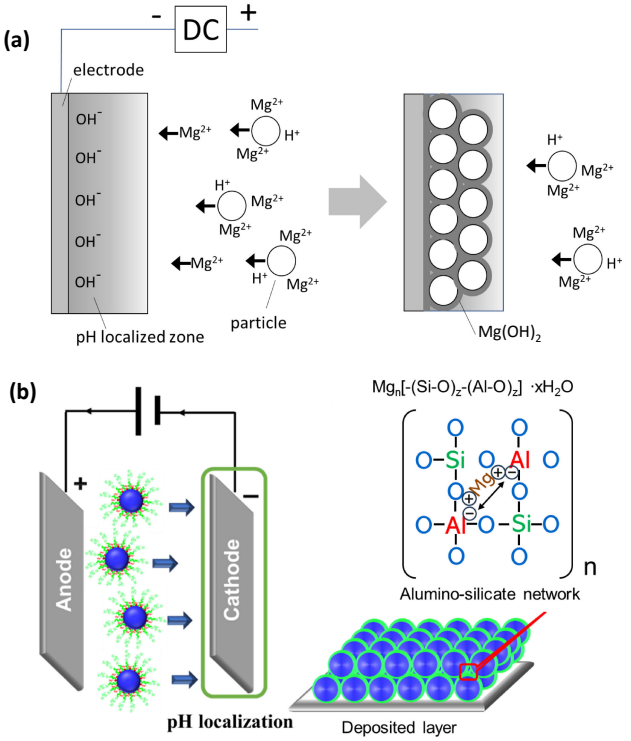

Fig. 5. Schematic diagram explaining the mechanism by which particles modified with (a) Mg ions and (b) Mg–Si–Al binder are firmly fixed on the cathode substrate.

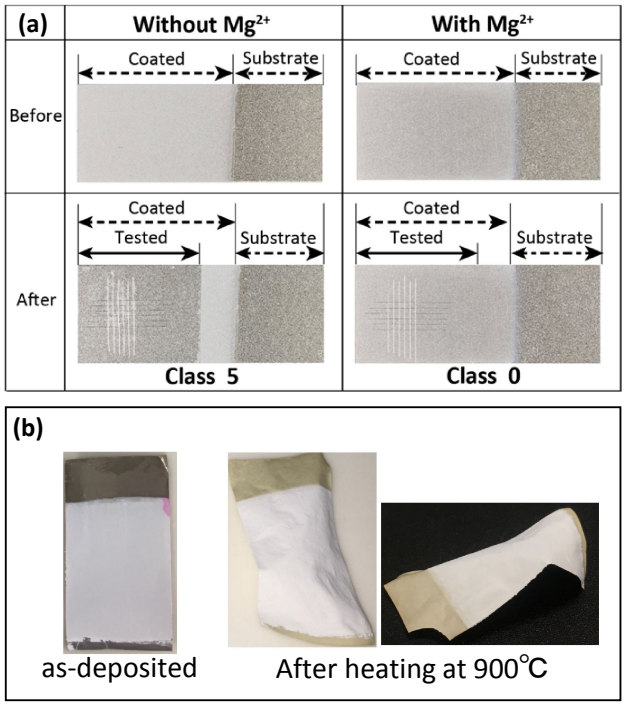

Fig. 6. (a) Effect of Mg ion on adhesion of HAp/Col coating layer on Ti plate. (b) Changes before and after heating of the coatings obtained from zirconia suspensions to which Mg–Si–Al-based inorganic binder was added.

the deposit becomes alkaline. Therefore, the authors focused on Mg as a substance that reacts with water and solidifies in an alkaline atmosphere.[26)–37)] **Figure 5** schematically shows the hydration reaction of Mg^{2+} ions or a Mg–Si–Al based inorganic binder solution near the cathode when an EPD coating is performed using a suspension in which Mg^{2+} ions or the Mg–Si–Al binder coexist.

Figure 6(a) shows an example of the EPD coating of a hydroxyapatite-collagen bone-like nanocomposite (HAp/Col) on a Ti substrate. In a suspension in which HAp/Col is dispersed in 2-PrOH (IPA) and a small amount of H_2O, $Mg(NO_3)_2{\cdot}H_2O$, and glycerol are added, the zeta potential significantly increases due to the presence of Mg^{2+}, and the stability of the suspension was significantly improved. Nevertheless, the coating layer after the EPD showed very good adhesion with no peeling off even in the subsequent tape test.[36)] It is probable that the Mg^{2+} ions adsorbed on the HAp/Col particles, giving them a positive surface charge, and also contributed to the formation of the hydroxide based on the following reaction.[28)]

$$Mg^{2+} + 2C_3H_7OH \rightarrow Mg(C_3H_7O)_2 + 2H^+ \quad (11)$$

$$Mg(C_3H_7O)_2 + 2H_2O \rightarrow Mg(OH)_2 + 2C_3H_7OH \quad (12)$$

In the absence of Mg^{2+}, the bonding between the Ti substrate and the HAp/Col particles and the bonding between the HAp/Col particles occur through van der Waals forces and liquid bridging forces originating from the residual solvent; therefore, this adhesive force is not that strong. However, when Mg^{2+} is added, a $Mg(OH)_2$ hydrogel is formed in the region near the cathode where the pH shifts to the alkaline side due to energization as shown in Fig. 5, this hydrogel acts as a binder. A crosslink was formed between the Ti substrate and the HAp/Col particles. This is probably the reason for the strong adhesion. Mg is known as an element that promotes bone formation and is eventually absorbed, so there are no disadvantages at all. This result has been developed into research on applying the HAp/Col coating to orthodontic anchorage devices.

Figure 6(b) shows an example of the EPD coating of 3 mol % Y-doped ZrO_2 (3Y-ZrO_2) on a Ti foil from a suspension of 3Y-ZrO_2 particles dispersed in the IPA solvent together with a compositionally-optimized Mg–Si–Al binder solution.[38)] The 3Y-ZrO_2 coating layer formed on the Ti substrate was extremely uniform, and even if the metal foil substrate was significantly deformed by subsequent heat treatment, it firmly adhered to the substrate surface without any cracks or peeling off. These results indicated that the Mg–Si–Al binder solution is very suitable even when heat treatment is required after film formation, and is also useful for ceramic heat-resistant coatings on metal surfaces. It was also confirmed that it is effective in uniformly coating ITO glass with a sialon phosphor film and coating a Ti substrate with bioglass.

In order to investigate the action mechanism of the Mg–Si–Al binder solution, ammonium hydroxide was added to the Mg–Si–Al binder solution to raise the pH to 10.4, the obtained gel-like material was dried at room temperature, then the crystal structure of the obtained powder was evaluated by XRD. As a result, it was found that the dried

product solidified at room temperature showed a high crystallinity, and its crystal structure was extremely similar to that of zeolite.[38] Based on this result, it was postulated that the Mg–Si–Al binder solution gels in the alkaline atmosphere near the cathode during the EPD process, wraps around the particles deposited on the cathode, thus contributing to substrate-particle and particle–particle bonding. The gelled product obtained at this time forms a three-dimensional network of aluminosilicate similar to a zeolite structure, and the Mg^{2+} ions are thought to play the role of charge compensation for the replacement of the Si sites with Al. Previous experiments by the authors have shown that cations other than Mg^{2+} ions have weak aggregation effects, but the reason for this has not yet been elucidated. The Mg–Si–Al binder solution can be used with or without heat treatment, and for coating various substrates, such as metal and ceramic substrates, making it suitable for EPD processes in fields where conventional organic binders are difficult to apply.

Generally, in the field of EPD processes, fine powders synthesized by wet methods have often been preferred, but if it is possible to use pulverized powders of substances synthesized by solid-phase reaction methods, the versatility of the EPD process will be significantly increased. However, when ball milling ceramic materials, contamination from the grinding media impairs particle dispersion, and fine powders ground to a submicron size have been considered unsuitable for colloidal processes. Therefore, an attempt was made to use wet-pulverized alumina powder and deposit it on stainless steel. As a result, it was found that a very good EPD film could be obtained by simply pulverizing, washing with water, diluting with IPA, and adding a Mg–Si–Al binder solution. In systems where contamination from ball milling is not a major problem, film formation was possible by simply diluting the wet-milled suspension in water with IPA and adding a Mg–Si–Al binder solution. The Mg–Si–Al binder solution enables the use of ball-milled powders, which have traditionally been avoided in the field of EPD processes, thus contributing to a significant increase in versatility.

4. Particle rearrangement in the post-EPD process

Research regarding the coagulation process of particles deposited on electrodes in the post-EPD processes is very limited. Sarkar et al. conducted SEM observations of monodispersed silica spheres deposited on a polished silicon wafer surface by EPD and concluded that the particles move and rearrange on the substrate, transforming into a two-dimensionally ordered close-packed state as the particle concentration increases.[39] However, there has been little discussion of how randomly-deposited particles on an electrode three-dimensionally consolidate in the post EPD process. It is generally known that colloidal particles dispersed in a liquid medium undergo a phase transition from a randomly arranged liquid phase state to a regularly arranged crystal phase state as the particle concentration increases. Therefore, in order to indirectly observe the three-dimensional rearrangement process of particles during the post-EPD process, we conducted the following experiment using monodispersed polystyrene (PS) spheres whose particle size is about the same as the wavelength of visible light.[40)–42)]

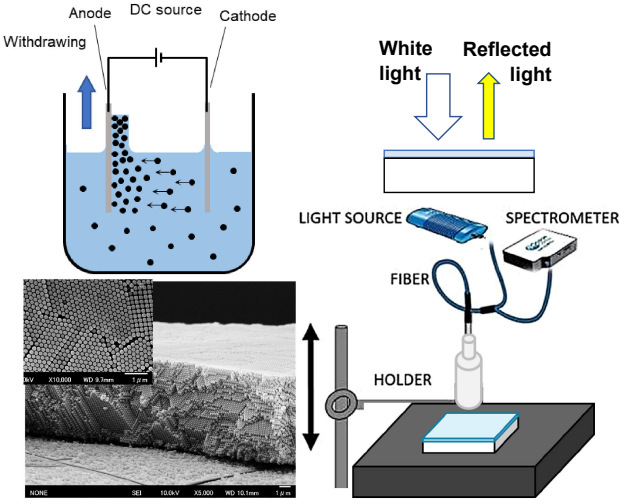

Fig. 7. Schematic diagram showing the experimental procedure for observing particle rearrangement from changes in the structural color during the drying process after EPD, and SEM photographs showing the surface and cross-sectional structures of colloidal crystals fabricated by the EPD method.

PS spheres (particle diameter 204.2 nm) synthesized by emulsion polymerization were dispersed in a mixed solvent of ethanol and water. Next, a DC electric field of 10 V/cm was applied to the suspension to deposit the negatively-charged PS spheres on an ITO glass anode. Furthermore, this film was pulled out of the suspension at a constant speed while applying the electric field, then immediately the substrate was placed horizontally and changes in the visible light reflection spectrum during room temperature drying were measured using a small optical fiber spectrometer. **Figure 7** shows a schematic diagram of the experimental procedure for observing particle rearrangement from changes in the structural color during the drying process after EPD, and SEM photographs showing the surface and cross-sectional structures of colloidal crystals fabricated by the EPD method.

Figures 8(a) and 8(b) show the changes in the reflectance spectra during the post-EPD process. The particle deposit layer immediately after removal showed a random arrangement with no Bragg diffraction peaks. However, about 10 s after lifting, a Bragg diffraction peak suddenly appeared, but then the peak gradually blue-shifted during the drying process. This result suggests that the particles are not yet ordered in the wet-deposited film immediately after EPD, but the particles become ordered during the subsequent solvent evaporation process. Finally, a film with a completed colloidal crystallization was obtained as shown in Fig. 7. This indicated the changes in the colloidal particles after EPD as shown in Fig. 8(c). In other words, it became clear that the effect of applying an electric field involved concentration of particles on the

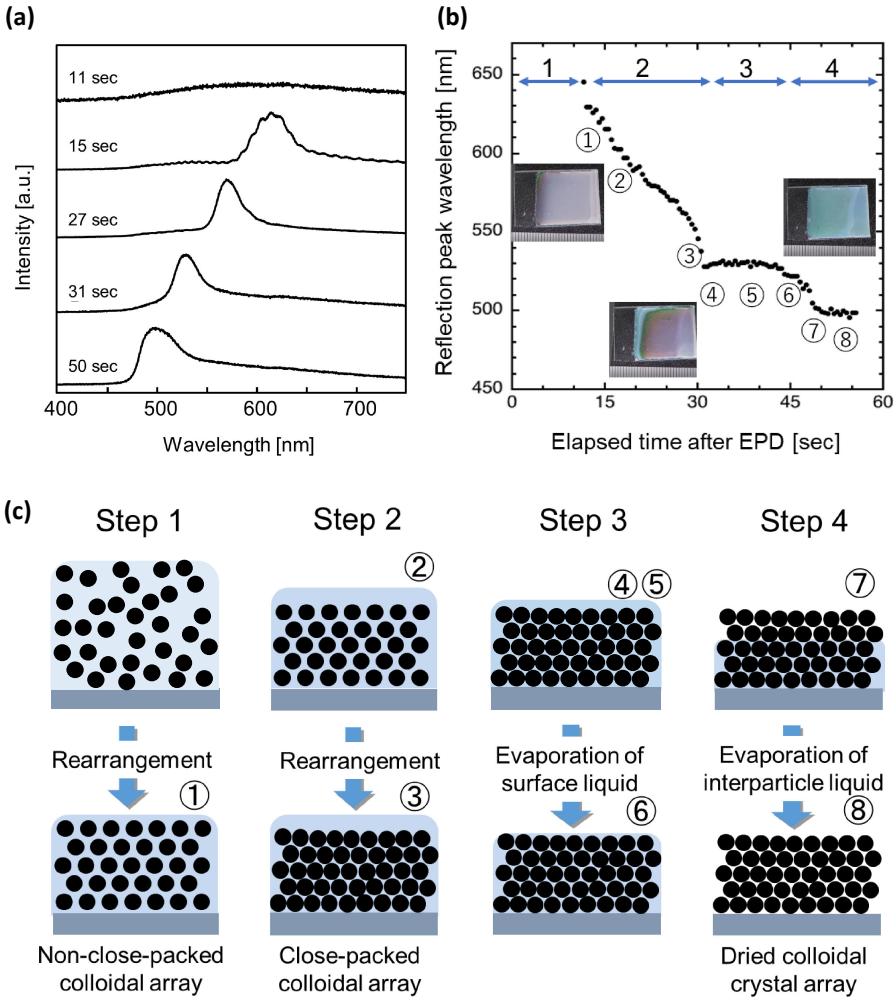

Fig. 8. (a) Appearance and peak change of reflectance spectrum associated with ordering process of colloidal particles during drying process of EPD film by visible light reflectance spectroscopy. (b) Schematic diagram showing the rearrangement and crystallization process of PS particles in the drying process immediately after EPD.

substrate. The crystallization of colloids is thought to be due to a crystal phase transition, i.e., "Alder transition", that accompanies particle rearrangement during the post-EPD drying process.[42)]

As already mentioned, during the EPD process, a high-density accumulation of charged particles in the liquid occurs due to the electric field, and charge loss and aggregation occur in the pH-biased solvent due to the electrode reaction. The particles in the dense aggregate continue to maintain the zeta potential necessary for electrostatic repulsion and are in an environment where they can rearrange as long as liquid is present. The EPD process has been shown to be highly effective as a rapid fabrication technique for colloidal crystal films that otherwise take hours to days to fabricate. Colloidal crystals have attracted attention as a novel material with unique optical properties whose structural color changes in response to the external environment, and is expected to be applied in various sensing fields. It is also easy to create inverse opal films using PS colloidal crystals as a template. **Figure 9** shows a tin oxide inverse opal film prepared using PS colloidal crystals as a template.

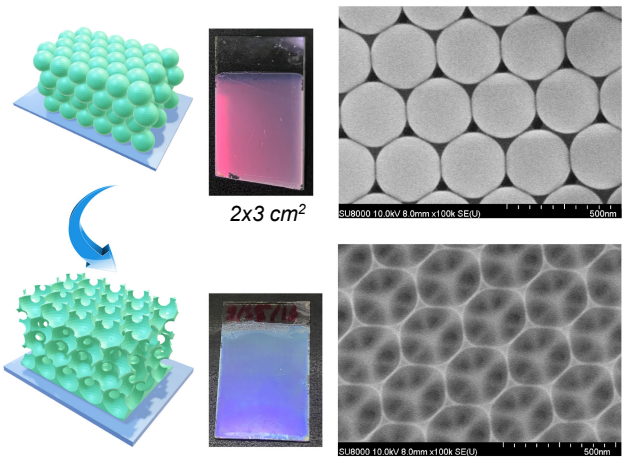

Fig. 9. Inverse opal film fabricated using polystyrene photonic crystal and tin precursor solution ($SnCl_4 \cdot 5H_2O$).

5. Manipulation of metal atom clusters by EPD

The EPD method is also very effective for manipulating single nanosized metal atom clusters.[43)–55)] Here, the synthesis of molybdenum hexa-atomic (Mo_6) cluster films by

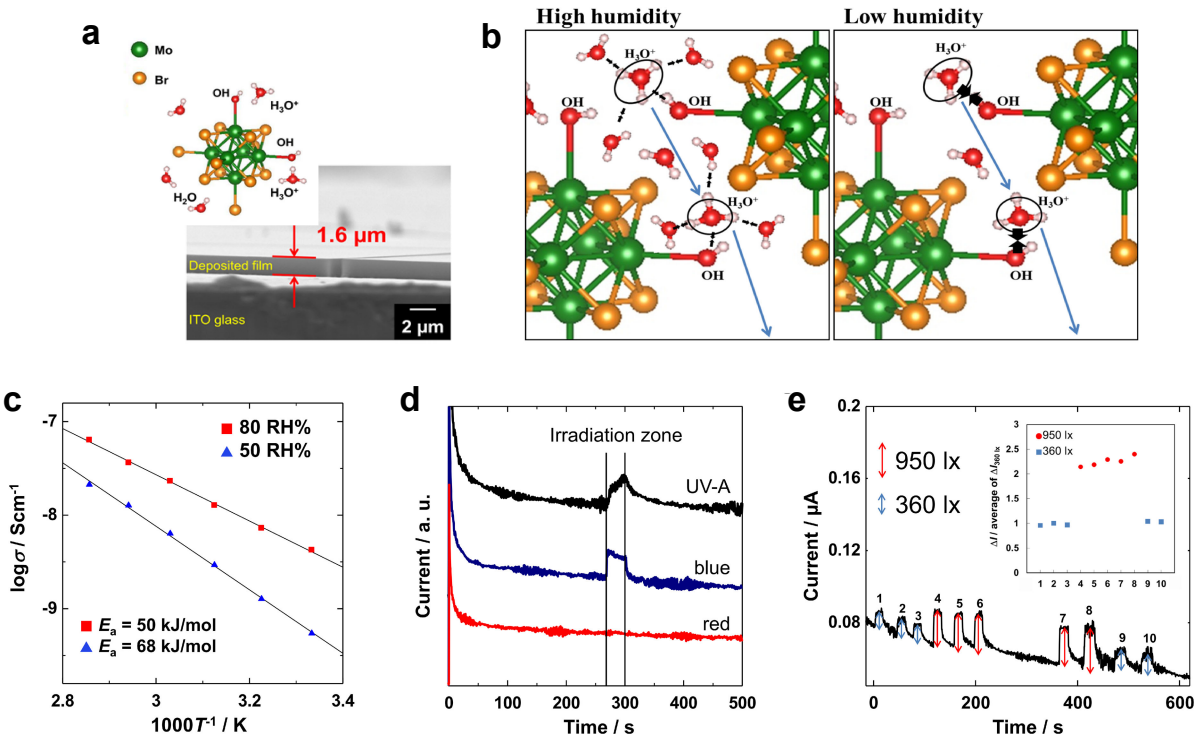

Fig. 10. Mo_6 cluster film formed on an ITO glass substrate by anodic EPD from a suspension of $Cs_2[\{Mo_6Br^i_8\}Br^a_6]$ clusters dispersed in acetone: (A) schematic diagram of the octahedral framework structure of the Mo_6 cluster unit and cross-sectional SEM photograph of the Mo_6 cluster film; (b) schematic diagram of the internal structure of the Mo_6 cluster film; (c) temperature and humidity dependence on proton conductivity; (d) irradiation light wavelength dependence on electron conductivity; (e) irradiation light intensity dependence on electron conductivity.

the EPD method is introduced. The optical properties of the Mo_6 clusters, such as light emission, absorption, and photocatalytic properties, which are expressed by their discrete electronic structure, have already been evaluated. However, little research has been conducted on their electrical properties because it is difficult to densely and uniformly solidify clusters, or to form them into a film. Very recently, we succeeded in forming a dense and uniform transparent cluster film on an ITO glass electrode from a Mo_6 cluster dispersion using the EPD method. We also succeeded in measuring the unique electrical properties of these Mo_6 cluster films, which change with the temperature, humidity, and light irradiation of different wavelengths and intensities.[52] **Figure 10**(a) shows the skeletal structure of the Mo_6 cluster unit and the cross-sectional view of the Mo_6 cluster film prepared by EPD from a $Cs_2[\{Mo_6Br^i_8\}Br^a_6]$ ($Cs_2Mo_6Br_{14}$) cluster suspension dispersed in acetone. XRD measurements did not show any peaks indicating a three-dimensional ordered structure in the cluster film, suggesting that the Mo_6 clusters were randomly packed. XRF analysis showed the absence of counter-cation Cs^+ in the cluster films. XPS, FT-IR and TOF-MS measurements showed that some of the Br apical ligands were substituted with OH, and H_3O^+ ions contributed to the stabilization of the Mo_6 cluster film as counter-cations. When solid-state synthesized $Cs_2Mo_6Br_{14}$ cluster powder is dispersed in a solvent, it dissociates into $[Mo_6Br_{14}]^{2-}$ ions, which have an octahedral skeletal structure, and Cs^+ ions, which are counter cations that stabilize the skeleton structure. When an electric field is applied to the colloidal solution, each species migrates to the electrodes of opposite polarity, so that in the Mo_6 cluster film, Cs^+ ions are completely replaced by H_3O^+ ions derived from trace water in the solvent. As a result, Mo_6 cluster films fabricated by the EPD process exhibit properties not found in films prepared by other processes such as dip coating or spin coating.

Figure 10(c) shows the electrical conductivity of the Mo_6 cluster film measured at different humidities (80 and 50 RH %) using the AC impedance method. The conductivity of the Mo_6 cluster film linearly increased with the increasing temperature. It was also found that the higher the humidity, the higher the conductivity, thus showing a humidity dependence. The activation energies were 50 and 67 kJ/mol at 80 and 50 RH %, respectively, consistent with the activation energies of the vehicle model using H_3O^+ ions as the carrier.

Based on the DC measurements, the trend of the current-time curve suggested ion conduction within the cluster membrane. When the cluster film is irradiated with ultraviolet LED light (390–395 nm) or blue LED light (465–475 nm) during DC measurement, a temporary increase in the current value is observed during the irradiation. On the other hand, no change in the current value is observed when irradiated with red LED light (665 nm) as shown in Fig. 10(d). Furthermore, as shown in Fig. 10(e), the

change in the current value became greater when the irradiation light was brighter. This phenomenon is interpreted to be because some of the excited electrons became conduction electrons. In other words, when Mo_6 clusters are deposited on a transparent electrode using the EPD method in an organic solvent containing a small amount of water, the water is incorporated into the cluster film. In this process, some of the ligand species that stabilize the framework structure of the Mo_6 clusters are partially substituted with hydroxyl groups, and the framework structure of the negatively charged Mo_6 cluster units is stabilized with hydronium ions as counter ions. The results revealed that the Mo_6 cluster film prepared using this method exhibited a mixed conduction of hydronium ions and electrons. Ionic conduction significantly changed depending on the atmospheric temperature and humidity, and electronic conduction significantly changed depending on the wavelength and intensity of the irradiated light. These unique multi-sensing properties are expected to bring new possibilities to environmental sensor applications that can simultaneously monitor the humidity and UV intensity. Research is also underway to develop a photoelectric conversion device in which Mo_6 clusters are supported in the voids of the above-mentioned inverse opal semiconductor film. Furthermore, using the EPD method, progress is being made in the development of a device for controlling light emission by supporting Mo_6 clusters in periodically arranged pore channels of an aluminum anodic oxide film with different pore sizes, densities, and shapes.[55] Studies regarding the manipulation of metal atom clusters using the EPD process have been extended to other metal species, such as tantalum hexa-atomic (Ta_6) clusters.

6. Conclusions

The EPD process is a film formation method that involves a chemical reaction in a liquid, unlike particle coating techniques such as spin coating and dip coating. A major advantage of the EPD method is that it can achieve superior functional properties that cannot be obtained by other deposition methods. There are great expectations for the development of EPD as a process for creating new functional materials.

Acknowledgments This research was mainly conducted at the National Institute for Materials Science (NIMS). I would like to express my sincere gratitude to all the researchers, postdocs, students, and laboratory staff at NIMS who worked hard to carry out this research. In particular, I would like to express my deepest gratitude to Dr. Chenning Zhang, Dr. Thi Kim Ngan Nguyen, Dr. Laxmidhar Besra, Dr. Masanori Kikuchi, Dr. Hiroshi Fudouzi, and Mr. Kenshi Harada.

References

1) I. A. Aksay, in "Advances in Ceramics, Vol. 9, Forming of Ceramics", Ed. by J. A. Mangels and G. L. Messing, American Ceramic Society, Columbus, OH (1984) pp. 94–104.
2) F. F. Lange, *J. Am. Ceram. Soc.*, 72, 3–15 (1989).
3) E. Carlström, in "Surface and Colloid Chemistry in Advanced Ceramics Processing", Ed. by R. J. Pugh and L. Bergström, Marcel Dekker, New York (1994) pp. 1–28.
4) J. A. Lewis, *J. Am. Ceram. Soc.*, 83, 2341–2359 (2000).
5) W. M. Sigmund, N. S. Bell and L. Bergström, *J. Am. Ceram. Soc.*, 83, 1557–1574 (2000).
6) P. S. Nicholson, P. Sarkar and D. De, Proc. Composites at Lake Louise '97 (1997) pp. 54–66.
7) P. Sarkar and P. S. Nicholson, *J. Am. Ceram. Soc.*, 79, 1987–2002 (1996).
8) O. O. Van der Biest and L. J. Vandeperre, *Annu. Rev. Mater. Sci.*, 29, 327–352 (1999).
9) A. R. Boccaccini and I. Zhitomirsky, *Curr. Opin. Solid St. M.*, 6, 251–260 (2002).
10) Y. Fukada, N. Nagarajan, W. Mekky, Y. Bao, H.-S. Kim and P. S. Nicholson, *J. Mater. Sci.*, 39, 787–801 (2004).
11) L. Besra and M. Liu, *Prog. Mater. Sci.*, 52, 1–61 (2007).
12) I. Corni, M. P. Ryan and A. R. Boccaccini, *J. Eur. Ceram. Soc.*, 28, 1353–1367 (2008).
13) B. Ferrari and R. Moreno, *J. Eur. Ceram. Soc.*, 30, 1069–1078 (2010).
14) T. Uchikoshi, in "Nanoparticle Technology Handbook", 2nd ed., Ed. by M. Hosokawa, K. Nogi, M. Naito and T. Yokoyama, Elsevier (2012) pp. 187–189.
15) T. Uchikoshi, T. S. Suzuki, H. Okuyama and Y. Sakka, *J. Mater. Res.*, 18, 254–256 (2003).
16) T. Uchikoshi, T. S. Suzuki, H. Okuyama and Y. Sakka, *J. Mater. Res.*, 19, 1487–1491 (2004).
17) T. Okamoto, S. Horii, T. Uchikoshi, T. S. Suzuki, Y. Sakka, R. Funahashi, N. Ando, M. Sakurai, J. Shimoyama and K. Kishio, *Appl. Phys. Lett.*, 89, 081912 (2006).
18) M. Suzuki, T. Uchikoshi, Y. Noguchi and M. Miyayama, *J. Electroceram.*, 24, 91–96 (2010).
19) T. Uchikoshi, T. S. Suzuki, H. Okuyama and Y. Sakka, *J. Eur. Ceram. Soc.*, 30, 1171–1175 (2010).
20) T. S. Suzuki, T. Uchikoshi, S. Sakakibara, H. Muto, A. Matsuda and Y. Sakka, *J. Ceram. Soc. Jpn.*, 119, 667–671 (2011).
21) H. C. Hamaker, *T. Faraday Soc.*, 35, 279–287 (1940).
22) D. De and P. S. Nicholson, *J. Am. Ceram. Soc.*, 82, 1151–2916 (2004).
23) L. Besra, T. Uchikoshi, T. S. Suzuki and Y. Sakka, *J. Eur. Ceram. Soc.*, 30, 1187–1193 (2010).
24) M. Mishra, S. Bhattacharjee, L. Besra, H. S. Sharma, T. Uchikoshi and Y. Sakka, *J. Eur. Ceram. Soc.*, 30, 2467–2473 (2010).
25) M. Mishra, Y. Sakka, T. Uchikoshi and L. Besra, *J. Ceram. Soc. Jpn.*, 121, 348–354 (2013).
26) J. A. Siracuse, J. B. Talbot, E. Sluzky and K. R. Hesse, *J. Electrochem. Soc.*, 137, 346–348 (1990).
27) M. J. Shane, J. B. Talbot, E. Sluzky and K. R. Hesse, *Colloid. Surface. A*, 96, 301–305 (1995).
28) B. E. Russ and J. B. Talbot, *J. Electrochem. Soc.*, 145, 1245–1252 (1998).
29) C. Zhang, T. Uchikoshi, T. Kitabatake and Y. Sakka, *Appl. Surf. Sci.*, 280, 229–234 (2013).
30) C. Zhang, T. Uchikoshi, T. Kitabatake, T. Nishimura, Y. Sakka and N. Hirosaki, *ECS Solid State Lett.*, 2, R23–R26 (2013).
31) C. Zhang, T. Uchikoshi, L. Liu, Y. Sakka and N.

Hirosaki, *Ceram. Int.*, 40, 8369–8375 (2014).
32) C. Zhang, T. Uchikoshi, L. Liu, Y. Sakka and N. Hirosaki, *Materials*, 7, 3623–3633 (2014).
33) C. Zhang, T. Uchikoshi, L. Liu, Y. Sakka and N. Hirosaki, *ECS J. Solid State Sc.*, 3, R195–R199 (2014).
34) C. Zhang, T. Uchikoshi, L. Liu and M. Kikuchi, *J. Electrochem. Soc.*, 116, D700–D706 (2019).
35) C. Zhang, T. Uchikoshi, L. Liu, C. Cai, J. Si and N. Hirosaki, *J. Am. Ceram. Soc.*, 103, 6780–6792 (2020).
36) K. Iwanami-Kadowaki, T. Uchikoshi, M. Uezono, M. Kikuchi and K. Moriyama, *J. Biomed. Mater. Res.*, 109, 1905–1911 (2021).
37) K. Katagiri, K. Uemura, R. Uesugi, N. Tarutani, K. Inumaru, T. Uchikoshi, T. Seki and Y. Takeoka, *ACS Appl. Mater. Inter.*, 12, 40768–40777 (2020).
38) C. Zhang and T. Uchikoshi, *Adv. Powder Technol.*, 34, 104236 (2023).
39) P. Sarkar, D. De, K. Yamashita, P. S. Nicholson and T. Umegaki, *J. Am. Ceram. Soc.*, 83, 1399–1401 (2000).
40) M. Koike, G. T. H. Tran, S. Azuma, H. Kiyono, T. Uchikoshi and H. Fudouzi, *J. Soc. Powder Technol. Jpn.*, 56, 339–346 (2019).
41) G. T. H. Tran, M. Koike, T. Uchikoshi and H. Fudouzi, *Adv. Powder Technol.*, 31, 3085–3668 (2020).
42) G. T. H. Tran, M. Koike, T. Uchikoshi and H. Fudouzi, *Langmuir*, 36, 10683–10689 (2020).
43) T. K. N. Nguyen, F. Grasset, B. Dierre, C. Matsunaga, S. Cordier, P. Lemoine, N. Ohashi and T. Uchikoshi, *ECS J. Solid State Sc.*, 5, R178–R186 (2016).
44) T. K. N. Nguyen, B. Dierre, F. Grasset, A. Renaud, S. Cordier, P. Lemoine, N. Ohashi and T. Uchikoshi, *J. Electrochem. Soc.*, 164, D412–D418 (2017).
45) T. K. N. Nguyen, B. Dierre, F. Grasset, N. Dumait, S. Cordier, P. Lemoine, A. Renaud, H. Fudouzi, N. Ohashi and T. Uchikoshi, *Coatings*, 7, 114 (2017).
46) T. K. N. Nguyen, A. Renaud, M. Wilmet, N. Dumait, S. Paofai, B. Dierre, W. Chen, N. Ohashi, S. Cordier, F. Grasset and T. Uchikoshi, *J. Mater. Chem. C*, 5, 10477–10484 (2017).
47) T. K. N. Nguyen, A. Renaud, B. Dierre, B. Bouteille, M. Wilmet, M. Dubernet, N. Ohashi, F. Grasset and T. Uchikoshi, *B. Chem. Soc. Jpn.*, 91, 1763–1774 (2018).
48) T. K. N. Nguyen, M. Dubernet, Y. Matsui, M. Wilmet, N. Shirahata, G. Rydzek, N. Dumait, M. Amela-Cortes, A. Renaud, S. Cordier, Y. Molard, F. Grasset and T. Uchikoshi, *Roy. Soc. Open Sci.*, 6, 181647 (2019).
49) A. Renaud, T. K. N. Nguyen, F. Grasset, M. Raissi, V. Guillon, F. Delabrouille, N. Dumait, P.-Y. Jouan, L. Cario, S. Jobic, Y. Pellegrin, F. Odobel, S. Cordier and T. Uchikoshi, *Electrochim. Acta*, 317, 737–745 (2019).
50) K. Kirakci, T. K. N. Nguyen, F. Grasset, T. Uchikoshi, J. Zelenka, P. Kubát, T. Ruml and K. Lang, *ACS Appl. Mater. Inter.*, 12, 52492–52499 (2020).
51) A. Renaud, P.-Y. Jouan, N. Dumait, S. Ababou-Girard, N. Barreau, T. Uchikoshi, F. Grasset, S. Jobic and S. Cordier, *ACS Appl. Mater. Inter.*, 14, 1347–1354 (2022).
52) K. Harada, T. K. N. Nguyen, F. Grasset, C. Comby-Zerbino, L. MacAleese, F. Chirot, P. Dugourd, N. Dumait, S. Cordier, N. Ohashi, M. Matsuda and T. Uchikoshi, *NPG Asia Mater.*, 14, 21 (2022).
53) T. K. N. Nguyen, C. Lebastared, M. Wilmet, N. Dumait, A. Renaud, S. Coedie, N. Ohashi, T. Uchikoshi and F. Grasset, *Sci. Technol. Adv. Mat.*, 23, 547–578 (2022).
54) T. K. N. Nguyen, F. Grasset, S. Cordier, N. Dumait, S. Ishii, H. Fudouzi and T. Uchikoshi, *Mater. Today Chem.*, 27, 101351 (2023).
55) T. K. N. Nguyen, H. Segawa, F. Grasset, S. Cordier, N. Dumait and T. Uchikoshi, *Mater. Lett.*, 15, 136144 (2024).

Tetsuo Uchikoshi is a Special Researcher of National Institute for Materials Science (NIMS) and a part-time lecturer at Hosei University. He received B.E. in Metallurgical Engineering (in 1986) and Ph.D. in Materials Science (in 1994) from Waseda University. He joined National Research Institute for Metals (NRIM), the predecessor of NIMS, as a researcher. After spending years as a senior researcher, a principal researcher, and a chief researcher, he was a group leader in 2011–2023. He was a visiting researcher at McMaster University in 1997–1998, a visiting professor at Kumamoto University in 2009–2012 and a guest professor at Hokkaido University in 2013–2023. His research specialty is the processing of various structural and functional ceramics using the charging characteristics of colloidal particles dispersed in liquid media.